

Constraints on the Bulk Lorentz Factors of GRB X-Ray Flares

Shuang-Xi Yi^{1,2}, Xue-Feng Wu^{3,4,5}, Fa-Yin Wang^{1,2} and Zi-Gao Dai^{1,2}

¹*School of Astronomy and Space Science, Nanjing University, Nanjing 210093, China;
dzg@nju.edu.cn*

²*Key Laboratory of Modern Astronomy and Astrophysics (Nanjing University), Ministry of
Education, China*

³*Purple Mountain Observatory, Chinese Academy of Sciences, Nanjing 210008, China*

⁴*Chinese Center for Antarctic Astronomy, Chinese Academy of Sciences, Nanjing, 210008, China*

⁵*Joint Center for Particle Nuclear Physics and Cosmology of Purple Mountain
Observatory-Nanjing University, Chinese Academy of Sciences, Nanjing 210008, China*

ABSTRACT

X-ray flares were discovered in the afterglow phase of gamma-ray bursts (GRBs) by the *Swift* satellite a decade ago and known as a canonical component in GRB X-ray afterglows. In this paper, we constrain the Lorentz factors of GRB X-ray flares using two different methods. For the first method, we estimate the lower limit on the bulk Lorentz factor with the flare duration and jet break time. In the second method, the upper limit on the Lorentz factor is derived by assuming that the X-ray flare jet has undergone saturated acceleration. We also re-estimate the initial Lorentz factor with GRB afterglow onsets, and find the coefficient of the theoretical Lorentz factor is 1.67 rather than the commonly used 2 for interstellar medium (ISM) and 1.44 for the wind case. We find that the correlation between the limited Lorentz factor and the isotropic radiation energy of X-ray flares in the ISM case is more consistent with that of prompt emission than the wind case in a statistical sense. For a comparison, the lower limit on Lorentz factor is statistically larger than the extrapolation from prompt bursts in the wind case. Our results indicate that X-ray flares and prompt bursts are produced by the same physical mechanism.

Subject headings: gamma ray: bursts - radiation mechanism: non-thermal

1. Introduction

Gamma-ray bursts (GRBs) are the most luminous explosive events in the Universe. It is well known that the observed gamma-ray emission are produced by relativistic outflows. The

fireball of a GRB is required to have a relativistic speed toward the earth in order to avoid the “compactness problem”. The Lorentz factor of the fireball increases with radius in the radiation-dominated acceleration phase. At the end of this phase, the fireball enters the matter-dominated coasting phase, which maintains a constant Lorentz factor (for reviews see Piran 1999; Zhang & Mészáros 2004; Mészáros 2006; Kumar & Zhang 2015). The Lorentz factor in the matter-dominated coasting phase, called the initial Lorentz factor, is a crucial parameter in understanding the physics of GRBs. There are several methods to constrain this initial Lorentz factor Γ_0 , but the most effective method is that the peak time of a GRB early afterglow onset is taken as the deceleration time of the outflow. An estimation of this initial value is possible by measuring the peak time of the afterglow light curve and the prompt isotropic energy $E_{\gamma,iso}$ (e.g., Molinari et al. 2007). This method was successfully applied in Liang et al. (2010) with a large sample of the early afterglow light curves. Liang et al. (2010) discovered a tight correlation between Γ_0 and $E_{\gamma,iso}$. In this paper, we re-estimate the initial Lorentz factor of GRBs in the ISM and wind cases, and also obtain a tight correlation between Γ_0 and $E_{\gamma,iso}$. The Γ_0 and $E_{\gamma,iso}$ correlation in the wind case is even more tighter than that of the ISM case.

X-ray flares are common phenomena in GRB X-ray afterglows in the *Swift* era. According to the temporal behavior and spectral properties of X-ray flares, it is widely argued that X-ray flares are produced by long-lasting central engine activities (Burrows et al. 2005; Ioka et al. 2005; Fan & Wei 2005; Falcone et al. 2006; Zhang et al. 2006; Wang & Dai 2013). It is generally believed that X-ray flares have the same physical origin as the prompt emission of GRBs. X-ray flares usually happen at $\sim 10^2 - 10^5$ s after prompt emissions, transferring a large percentage of the outflow energy to the radiation. Most of the methods proposed to constrain the initial Lorentz factor of GRBs are not suitable for X-ray flares. Since the fluence of most X-ray flares are smaller than the prompt emission, their energies and Lorentz factors are supposed to be smaller than those of GRBs. In this paper, we use two different methods to place limits on the Lorentz factor of X-ray flares. In Section 2, we introduce the method to estimate of the initial Lorentz factor Γ_0 of GRBs. The two methods of constraining the X-ray flares Lorentz factors are shown in Section 3. Sample study are presented in Section 4, and our results are summarized and discussed in Section 5. A concordance cosmology with parameters $H_0 = 71 \text{ km s}^{-1} \text{ Mpc}^{-1}$, $\Omega_M = 0.30$, and $\Omega_\Lambda = 0.70$ are adopted. Notation Q_n denotes $Q/10^n$ in the cgs units throughout the paper.

2. Estimating the Initial Lorentz Factor Γ_0

When a relativistic fireball shell sweeps up the circumburst medium, two shocks appear: a reverse shock propagating into the fireball shell, and a forward shock propagating into the ambient medium. We suppose that the fireball shell and two shocks are spherical. Physical quantities

denoted by “ r ” are defined in the co-moving frame. We divide this two-shock system into 4 regions (Sari & Piran 1995; Yi et al. 2013): (1) The unshocked ambient medium (n_1, e_1, p_1, Γ_1), (2) the shocked ambient medium ($n'_2, e'_2, p'_2, \Gamma_2$), (3) the shocked fireball shell ($n'_3, e'_3, p'_3, \Gamma_3$), and (4) the unshocked fireball shell ($n'_4, \Gamma_4 = \Gamma_0$), where n is the number density, e is the internal energy density, p is the pressure, and Γ is the bulk Lorentz factor. Hereafter we calculate the properties of the reverse shock emission at the radius R_\times , where the reverse shock finishes crossing the ejecta shell and the Lorentz factor of the shell is Γ_\times .

The assumptions of the equilibrium of pressures and equality of velocities along the contact discontinuity lead to $p'_2 = p'_3$ and $\Gamma_2 = \Gamma_3$, respectively. With the jump condition for the shocks and the equilibrium of pressures, we can obtain,

$$(4\Gamma_{34} + 3)(\Gamma_{34} - 1)n'_4 = (4\Gamma_2 + 3)(\Gamma_2 - 1)n_1. \quad (1)$$

The Lorentz factor of the reverse shock Γ_{34} could be approximated as

$$\Gamma_{34} = \frac{1}{2} \left(\frac{\Gamma_3}{\Gamma_4} + \frac{\Gamma_4}{\Gamma_3} \right) = \frac{1}{2} \left(\frac{\Gamma_4^2 + \Gamma_3^2}{\Gamma_4 \Gamma_3} \right), \quad (2)$$

as long as $\Gamma_3 \gg 1$ and $\Gamma_4 \gg 1$. Substituting Equation (2) into Equation (1), we can obtain the following equation

$$\frac{(\Gamma_4 - \Gamma_3)^2}{\Gamma_4 \Gamma_3} \left[\frac{(\Gamma_4 + \Gamma_3)^2}{\Gamma_4 \Gamma_3} - \frac{1}{2} \right] n'_4 = 4\Gamma_3^2 n_1. \quad (3)$$

Because $\Gamma_3 \gg 1$, $\Gamma_4 \gg 1$ and $\Gamma_4 \geq \Gamma_3$, we ignore the constant 1/2 term in the Equation (3) and thus we can obtain the solution of this equation (ignoring the negative solution, also see Panaitescu & Kumar 2004)

$$\Gamma_3 = \frac{\Gamma_4}{\left[1 + 2\Gamma_4 (n_1/n'_4)^{1/2} \right]^{1/2}}. \quad (4)$$

Here we obtain the relation between the Lorentz factor of shocked fireball shell Γ_3 and the initial Lorentz factor Γ_0 (Γ_4), which depends on the ratio of these two comoving densities. The number density of the ambient medium is assumed to be $n_1 = AR^{-k}$ (Dai & Lu 1998; Mészáros et al 1998; Chevalier & Li 2000; Wu et al 2003, 2005; Yi et al. 2013), such a circumburst medium is a homogeneous interstellar medium (ISM) for $k = 0$, and a typical stellar wind environment for $k = 2$. The fireball shell is characterized by an initial kinetic energy E_k , initial Lorentz factor Γ_4 , and a width Δ in the lab frame attached to the explosion center, so the number density of the shell in the comoving frame is $n'_4 = E_k / (4\pi m_p c^2 R^2 \Delta \Gamma_4^2)$. The ratio of the comoving number density of the relativistic shell n'_4 to the number density of the ambient medium n_1 defined in Sari & Piran (1995) is

$$f = \frac{n'_4}{n_1} = \frac{E_k}{4\pi A m_p c^2 \Delta \Gamma_4^2 R^{2-k}} = \frac{X}{\Delta \Gamma_4^2 R^{2-k}}, \quad (5)$$

where $X = E_k/(4\pi Am_p c^2)$. The difference between the lab frame speed of the unshocked fireball shell and that of the reverse shock is (Kumar & Panaitescu 2003),

$$\beta_4 - \beta_{RS} = \frac{1.4}{\Gamma_4^2} \left(\frac{\Gamma_4^2 n_1}{n'_4} \right)^{\frac{1}{2}} = \frac{1.4}{\Gamma_4} \left(\frac{1}{f} \right)^{\frac{1}{2}}. \quad (6)$$

Considering the thin shell case $\Delta \simeq R/(2\Gamma_4^2)$, we can calculate the radius R_\times where the reverse shock finishes crossing the fireball shell,

$$\Delta(R_\times) = \int_0^{R_\times} (\beta_4 - \beta_{RS}) dR. \quad (7)$$

The substitution of Equation (5) and (6) into Equation (7) leads to

$$R_\times = \left[\frac{2(5-k)^2 X}{5.6^2 \Gamma_4^2} \right]^{\frac{1}{3-k}} = \left[\frac{(5-k)^2 E_k}{2 \times 5.6^2 \pi A m_p c^2 \Gamma_4^2} \right]^{\frac{1}{3-k}}. \quad (8)$$

So the comoving density ratio at R_\times is

$$f_\times = \frac{n'_4}{n_1} = \frac{2X}{R_\times^{3-k}} = \frac{5.6^2}{(5-k)^2} \Gamma_4^2. \quad (9)$$

Substituting Equation (9) into Equation (4), we can obtain the Lorentz factor of the reverse shock as it finishes crossing the shell

$$\Gamma_\times = \frac{\Gamma_4}{\left[1 + 2\Gamma_4 (R_\times^{3-k}/(2X))^{1/2} \right]^{1/2}} = \frac{\Gamma_4}{[1 + 0.357(5-k)]^{1/2}}. \quad (10)$$

Therefore, the relation between Γ_\times and the initial Lorentz factor Γ_0 is

$$\Gamma_\times = 0.60 \Gamma_0, \text{ for } k = 0 \text{ (ISM)}, \quad (11)$$

and

$$\Gamma_\times = 0.70 \Gamma_0, \text{ for } k = 2 \text{ (Wind)}. \quad (12)$$

For the thin shell case, the reverse shock crossing time T_\times is almost corresponding to the deceleration time T_{dec} , i.e., $T_\times \sim T_{dec}$. Therefore, we can derive the initial Lorentz factor in the ISM and wind type cases (also see Panaitescu & Kumar 2004). For $k = 0$ (ISM),

$$\Gamma_0 = \frac{1}{0.60} \Gamma_\times = 1.67 \left[\frac{3E_{\gamma,iso}}{32\pi n_1 m_p c^5 \eta t_{p,z}^3} \right]^{\frac{1}{8}}, \quad (13)$$

and for $k = 2$ (wind),

$$\Gamma_0 = \frac{1}{0.70} \Gamma_\times = 1.44 \left[\frac{E_{\gamma,iso}}{8\pi A m_p c^3 \eta t_{p,z}} \right]^{\frac{1}{4}}. \quad (14)$$

With the isotropic-equivalent energy $E_{\gamma,iso}$ and the peak time of the afterglow onset $t_{p,z}$, we can estimate the initial Lorentz factor of GRBs, where $t_{p,z} = t_p/(1+z)$. Liang et al. (2010) discovered a tight correlation between Γ_0 and $E_{\gamma,iso}$ using 20 GRBs which show deceleration feature in the early afterglow light curves. Other work also confirmed this correlation, but with different methods and power-law indices (Ghirlanda et al. 2012; Lü et al. 2012). Using the data of $t_{p,z}$ and $E_{\gamma,iso}$ from Liang et al. (2010, 2013) and Lü et al. (2012), we re-constrain the initial Lorentz factor, and also discover a tight Γ_0 and $E_{\gamma,iso}$ correlation for the ISM and wind cases. The Γ_0 and $E_{\gamma,iso}$ correlation in the wind case is even more tighter than that in the ISM case, as shown in Figs. 4 and 5.

3. Methods of Constraining the Bulk Lorentz Factor of X-ray flares

Because most of the models estimating the bulk Lorentz factor during the GRB prompt emission phase are inapplicable for the X-ray flares, we introduce two methods to constrain the upper and lower limits on the Lorentz factor of X-ray flares in this section. In principle, GRB outflows could be structured, but we suppose that the outflows are conical (also called jet-like) and the half-opening angles of the outflows have a same/constant value in a single GRB, i.e., the half-opening angle of the X-ray flare jet is the same as that of the prompt jet in one GRB. Therefore, we suppose that each X-ray flare is produced in a conical uniform jet with half-opening angle θ_j . If there are several flares in one X-ray afterglow, we also assume these X-ray flares have the same jet half-opening angle θ_j .

Method I: Lower limit on the Lorentz factor of X-ray flares. We use the late internal shock emission model to constrain the lower limits of the Lorentz factor of X-ray flares (Wu et al. 2006, 2007). The quick decline of X-ray flares after the peak time is widely interpreted as the high latitude component of X-ray pulses (Burrows et al. 2005; Tagliaferri et al. 2005; Zhang et al. 2006; Nousek et al. 2006; Liang et al. 2006). Wu et al. (2007) supposed that emission from the same internal shock radius R_{int} but with different angles would have different arrival times to the observer, which is due to light propagation effect. The delay time of different photons with different θ ($\theta < \theta_j$) is

$$\Delta T = \frac{R_{int}(1 - \cos \theta)}{c}. \quad (15)$$

If photons are emitted at an angle $\theta = \theta_j$, then the delay time ΔT is about the duration time of the X-ray flare. We denote the timescale of the decay part of an X-ray flare by T_{decay} . We could put forth a constraint on the decaying timescale of the flare and the jet-opening angle, i.e.

$$T_{decay} < \frac{R_{int}(1 - \cos \theta_j)}{c}. \quad (16)$$

Another timescale is the angular spreading variability time T_{rise} , which is the rise time of an X-ray flare,

$$T_{rise} = \frac{R_{int}(1 - \cos(1/\Gamma_x))}{c} \approx \frac{R_{int}}{2\Gamma_x^2 c}. \quad (17)$$

Combining the decaying timescale and rising timescale, we could get a lower limit on the Lorentz factor of each X-ray flare,

$$\Gamma_x > \left(\frac{T_{decay}}{T_{rise}} \right)^{\frac{1}{2}} \left[\frac{1}{2(1 - \cos \theta_j)} \right]^{\frac{1}{2}} \approx \theta_j^{-1} \left(\frac{T_{decay}}{T_{rise}} \right)^{\frac{1}{2}}. \quad (18)$$

With the jet opening angle θ_j , decaying timescale and rising timescale, we can constrain the lower limit of the Lorentz factor of each X-ray flare. The jet half-opening angle θ_j can be estimated from the late afterglow of a GRB if there is a jet break in the afterglow light curve. So, we selected GRBs which have jet breaks and flares in the X-ray afterglow light curve in our sample. The sample is listed in Table 1.

Method II: Upper limit on the Lorentz factor of X-ray flares. The physical mechanism of X-ray flares is still unclear. X-ray flares are known to be similar to those of prompt emission pulses through studying of the temporal behavior and energy spectrum (Chincarini et al. 2010). We generally consider X-ray flares having the same physical origin as the prompt emission of GRB, and they are all due to the long-lasting activity of the central engine (Fan & Wei 2005; Zhang et al. 2006). But there is still controversy about the origin of X-ray flares of GRBs. X-ray flares of short GRBs can be produced by differentially rotating, millisecond pulsars from the mergers of binary neutron stars (Dai et al. 2006). Magnetic reconnection-driven explosions lead to multiple X-ray flares minutes after the prompt GRB. Wang & Dai (2013) performed a statistical study of X-ray flares for long and short GRBs, and found energy, duration, and wait-time distributions similar to those of solar flares, which indicates that X-ray flares of GRBs may be powered by magnetic reconnection. According to the standard GRB fireball model, after the initial radiation-dominated acceleration phase, the fireball enters the matter-dominated “coasting” phase (Piran 1999; Mészáros 2002; Zhang & Mészáros 2004). Whether the fireball is baryon-rich or not determines how long is the initial radiation-dominated acceleration phase. If the fireball is baryon-poor, the initial energy of the fireball will be quickly converted into radiation energy and produce bright and brief thermal emission, which is inconsistent with most of the observations. The spectra of X-ray flares are typically non-thermal, with a photon index of about ~ -2.0 (Falcone et al. 2007). This suggests that X-ray flares happen when the jet is optically thin. Meanwhile, thermal emission just before any X-ray flare with compatible flux has never been detected, indicating that the jet responsible for the flare attains saturated acceleration. This requires baryon loading in the jet to be large enough, or that the Lorentz factor has an upper limit. On the other hand, the upper limit on the Lorentz factor

of an X-ray flare can be estimated as (Jin et al. 2010)

$$\Gamma_x \leq \left(\frac{L \sigma_T}{8\pi m_p c^3 R_0} \right)^{\frac{1}{4}}, \quad (19)$$

which depends on the total luminosity L and initial radius R_0 of the flare outflow. Jin et al. (2010) assumed that the observed X-ray flare luminosity is just a fraction ($\epsilon_x = 0.1$) of the total luminosity of the outflow, that is $L_x = 0.1L$ (also see, Fan & Piran 2006). R_0 is taken to be 10^7 cm, which is comparable to the radius of a neutron star. $R_0 = 10^7$ cm is a conservative value, in some cases, R_0 is taken to be $\sim 10^8$ cm or even larger (Pe’er et al. 2007). With the proper values, we are able to get an upper limit on Γ_x . In our sample, L_x is taken as $E_{x,iso}/T_{90,x}$, where $E_{x,iso}$ and $T_{90,x}$ are the isotropic energy and duration time of one flare respectively. The redshift of those GRBs in our sample are all measured, the isotropic 0.3 - 10 keV energy of the X-ray flares in the sample can be estimated from the fluence as

$$E_{x,iso} = \frac{4\pi D_L^2}{1+z} S_x, \quad (20)$$

where S_x is the fluence of an X-ray flare.

4. Case Studies

Our method for placing lower limits on the Lorentz factor is feasible if the X-ray light curve presents flare and jet break simultaneously. Our sample consists of 20 GRBs with X-ray flares, redshift and jet break time (Falcone et al. 2007; Chincarini et al. 2010; Bernardini et al. 2011; Lu et al. 2012). Some of them have several flares in one GRB. The total number of X-ray flares is 43. We assume that the opening angle is the same for the jets responsible for prompt emission and late X-ray flares in a single GRB. According to the appearance time of X-ray flares, we mark the corresponding numerical order, which can be seen in the Table 1. The T_{rise} , T_{decay} , S_x , and $T_{90,x}$ of each flare are reported in Falcone et al. (2007), Chincarini et al. (2010) and Bernardini et al. (2011). θ_j^{Wind} and θ_j^{ISM} are calculated with the data taken from Lu et al. (2012) when the Eq. (22) and Eq. (23) are applied. The Lorentz factor in the wind type circumburst media is (Chevalier & Li 2000)

$$\Gamma = 5.9 \left(\frac{1+z}{2} \right)^{1/4} E_{k,52}^{1/4} A_*^{-1/4} t_{days}^{-1/4}, \quad (21)$$

where $E_{k,52}$ is the initial kinetic energy of the fireball shell in units of 10^{52} ergs, t_{days} is the observer’s time in units of days, $A = \dot{M}_w / 4\pi V_w = 5 \times 10^{11} A_* \text{ g cm}^{-1}$ is the wind parameter, \dot{M}_w is the wind mass-loss rate, and V_w is the wind velocity. Because the jet break effects are considered when

$\Gamma \approx \theta_j^{-1}$, so Equation (21) could be used to estimate the jet half-opening angle for the wind case,

$$\theta_j^{wind} = 0.12 \text{ rad} \left(\frac{T_j}{1 \text{ day}} \right)^{1/4} \left(\frac{1+z}{2} \right)^{-1/4} E_{\gamma,iso,52}^{-1/4} \left(\frac{\eta}{0.2} \right)^{1/4} A_*^{1/4}. \quad (22)$$

where η is the efficiency of prompt GRBs and $A_* = 1$ adopted in this paper. The jet half-opening angle in the interstellar medium case could be described by (Sari et al. 1999; Rhoads 1999; Frail et al. 2001; Yi et al. 2015),

$$\theta_j^{ISM} = 0.076 \text{ rad} \left(\frac{T_j}{1 \text{ day}} \right)^{3/8} \left(\frac{1+z}{2} \right)^{-3/8} E_{\gamma,iso,53}^{-1/8} \left(\frac{\eta}{0.2} \right)^{1/8} \left(\frac{n}{1 \text{ cm}^{-3}} \right)^{1/8}. \quad (23)$$

The distribution of jet half-opening angles for the ISM and wind cases is shown in Fig 1.

We assume that X-ray flares are coming from relativistic jets. The tail of an X-ray flare is interpreted as emission from high latitude areas of the jet. The duration of the flare is determined by the half-opening angle of the jet through the curvature effect. With the jet half-opening angle θ_j estimated from the jet break time, decaying timescale and rising timescale of the flare, we can obtain the lower limit on the Lorentz factor of the flare via Equation (18). The upper limit on the Lorentz factor is determined by the total luminosity and initial radius of the outflow. The observed average luminosity is obtained from the isotropic 0.3 - 10 keV energy of the X-ray flare averaged by the duration time of the flare. The total luminosity of the flare is assumed to be 10 times of the observed X-ray luminosity. As already mentioned, the initial radius of the outflow R_0 is taken as 10^7 cm. The obtained limits on the bulk Lorentz factor of X-ray flares range from tens to hundreds, as can be seen in Fig 2 and 3. We find that in the ISM case the correlation between the Lorentz factor and the isotropic radiation energy of X-ray flares is almost consistent with that of prompt emission of GRBs (Fig 4). However, in the wind case the lower limit on the Lorentz factor is statistically larger than the extrapolation from prompt bursts (Fig 5).

5. Discussion

X-ray flares are common features in GRB X-ray afterglows, and most of them have occurred at the early period. We can conclude that all the flares in our sample occurred before the jet break, which can be seen from the Table 1. Here, we define $f = \theta_{j,\gamma}/\theta_{j,x}$, where $\theta_{j,x}$ is the half-opening angle of the X-ray flare jet while $\theta_{j,\gamma}$ is the half-opening angle of the jet responsible for prompt emission. If $f = 1$, one suggests that the jet may be conical and the flare jet and prompt emission jet have the same half-opening angle as we discussed above. The jet opening angle might be larger during the prompt emission and smaller for the X-ray flares, i.e., $f > 1$, which has been predicted in some models with magnetic-dominated jets (Levinson & Begelman 2013; Bromberg et al. 2014).

In this case, the lower limit of flare Lorentz factor would be larger than that estimated with Eq. (18) assuming $\theta_{j,x} = \theta_{j,\gamma}$. The corresponding lower limits on X-ray flare Lorentz factor in Figs. 4 and 5 will increase by a factor of f , making the X-ray flares possibly more inconsistent (especially for the wind case) with the extrapolation of the correlation between isotropic radiation energy and Lorentz factor of prompt emission of GRBs. On the other hand, although several observations suggest that in some GRBs the ejecta may have large scale magnetic fields and therefore the ejecta could be magnetized, the degree of magnetization is usually estimated as $\sigma < \text{a few}$ in the afterglow phase. So in this paper we assume that for simplicity GRB jets have negligible magnetization, and the outflows have same half-opening angle ($f = 1$) in one GRB.

In addition, the fluence of most X-ray flares are smaller than that of prompt emission, their energies and Lorentz factors are supposed to be smaller than those of GRBs. The initial Lorentz factor of GRBs in this paper is generally larger than a few hundreds, and it is always larger than the lower limits of X-ray flare Lorentz factor in the same GRB. In Fig 6, we plot 5 GRBs having prompt and flare Lorentz factors, GRBs 050820A, 060418, 060906, 070318, and 071031. The initial Lorentz factors of these 5 GRBs are generally much larger than the lower limits of the Lorentz factor of their X-ray flares, and usually smaller than the upper limits of flare Lorentz factors.

6. Conclusion

The initial Lorentz factor is a key parameter to understanding the GRB physics. In this paper, we have re-estimated the initial Lorentz factor in a more accurate way. From Equation (13), we obtain a coefficient 1.67 for the ISM case, instead of 2 adopted in previous literature. We also constrain the initial Lorentz factor in the wind case, which is shown as Equation (14). With the estimated initial Lorentz factors in this paper, we confirm the tight correlation between the initial Lorentz factor and isotropic energy of GRBs for the ISM case. There is an even tighter correlation between the initial Lorentz factor and isotropic energy of GRBs for the wind case.

Our sample consists of 20 GRBs with X-ray flares, whose redshifts and jet break times are known. Some of them have several flares. The total number of X-ray flares in our sample is 43. We assume that the half-opening angle is the same for the jets responsible for prompt emission and late X-ray flares in one GRB. Our results are shown in Fig 4 (ISM) and Fig 5 (Wind), which also show the correlation between isotropic radiation energy and the Lorentz factor of prompt emission of GRBs. The obtained limits on the bulk Lorentz factor of X-ray flares range from a few tens to hundreds, together with the isotropic radiation energy, are generally consistent with the correlation for prompt GRBs for the ISM case. Our results indicate that X-ray flares and prompt bursts may be caused by the same mechanism, as both are produced by the long-lasting activity of the central

engine. However, in the wind case the lower limit on Lorentz factor is statistically larger than the extrapolation from prompt bursts.

We thank the anonymous referee for constructive suggestions. We also thank Bing Zhang, En-Wei Liang, Yun-Wei Yu, Liang-Duan Liu, Di Xiao and A-Ming Chen for useful comments and helps. This work is supported by the National Basic Research Program (“973” Program) of China (grant Nos. 2014CB845800 and 2013CB834900), the program A for Outstanding PhD candidate of Nanjing University, and the National Natural Science Foundation of China (grant Nos. 11033002, 11422325, 11373022 and 11322328). X.F.W was also partially supported by the One-Hundred-Talent Program, the Youth Innovation Promotion Association, and the Strategic Priority Research Program “The Emergence of Cosmological Structure” (grant No. XDB09000000) of the Chinese Academy of Sciences, and the Natural Science Foundation of Jiangsu Province (No. BK2012890). F.Y.W was also partially supported by the Excellent Youth Foundation of Jiangsu Province (BK20140016).

REFERENCES

- Bernardini, M. G., Margutti, R., Chincarini, G., Guidorzi, C., & Mao, J. 2011, *A&A*, 526, AA27
- Bromberg, O., Granot, J., Lyubarsky, Y., & Piran, T. 2014, *MNRAS*, 443, 1532
- Burrows, D. N., Romano, P., Falcone, A., et al. 2005, *Science*, 309, 1833
- Chevalier, R. A., & Li, Z. Y. 2000, *ApJ*, 536, 195
- Chincarini, G., Mao, J., Margutti, R., et al. 2010, *MNRAS*, 406, 2113
- Dai, Z. G., & Lu, T. 1998, *MNRAS*, 298, 87
- Dai, Z. G., Wang, X. Y., Wu, X. F., & Zhang, B. 2006, *Science*, 311, 1127
- Falcone, A. D., Burrows, D. N., Lazzati, D., et al. 2006, *ApJ*, 641, 1010
- Falcone, A. D., Morris, D., Racusin, J., et al. 2007, *ApJ*, 671, 1921
- Fan, Y. Z., & Wei, D. M. 2005, *MNRAS*, 364, L42
- Fan, Y., & Piran, T. 2006, *MNRAS*, 369, 197
- Frail, D. A., Kulkarni, S. R., Sari, R., et al. 2001, *ApJ*, 562, L55
- Ghirlanda, G., Nava, L., Ghisellini, G., et al. 2012, *MNRAS*, 420, 483
- Ioka, K., Kobayashi, S., & Zhang, B. 2005, *ApJ*, 631, 429
- Jin, Z. P., Fan, Y. Z., & Wei, D.-M. 2010, *ApJ*, 724, 861
- Kumar, P., & Panaitescu, A. 2003, *MNRAS*, 346, 905
- Kumar, P., & Zhang, B. 2015, *Physics Report*, 561, 1
- Lü, J., Zou, Y. C., Lei, W. H., et al. 2012, *ApJ*, 751, 49
- Levinson, A., & Begelman, M. C. 2013, *ApJ*, 764, 148
- Liang, E. W., Zhang, B., O’Brien, P. T., et al. 2006, *ApJ*, 646, 351
- Liang, E. W., Li, L., Gao, H., et al. 2013, *ApJ*, 774, 13
- Liang, E. W., Yi, S. X., Zhang, J., et al. 2010, *ApJ*, 725, 2209
- Lu, R. J., Wei, J. J., Liang, E. W., et al. 2012, *ApJ*, 756, 112

- Mészáros, P. 2002, ARAA, 40, 137
- Mészáros, P. 2006, Rep. Prog. Phys., 69, 2259
- Mészáros, P., Rees, M. J., & Wijers, R. A. M. J. 1998, ApJ, 499, 301
- Molinari, E., Vergani, S. D., Malesani, D., et al. 2007, A&A, 469, L13
- Nousek, J. A., Kouveliotou, C., Grupe, D., et al. 2006, ApJ, 642, 389
- Panaiteanu, A., & Kumar, P. 2004, MNRAS, 353, 511
- Pe’er, A., Ryde, F., Wijers, R. A. M. J., Mészáros, P., & Rees, M. J. 2007, ApJ, 664, L1
- Piran, T. 1999, Phys. Rep., 314, 575
- Rhoads, J. E. 1999, ApJ, 525, 737
- Sari, R., & Piran, T. 1995, ApJ, 455, L143
- Sari, R., Piran, T., & Halpern, J. P. 1999, ApJ, 519, L17
- Tagliaferri, G., Goad, M., Chincarini, G., et al. 2005, Nature, 436, 985
- Wang, F. Y., & Dai, Z. G. 2013, Nature Physics, 9, 46
- Wu, X. F., Dai, Z. G., Huang, Y. F., & Lu, T. 2005, ApJ, 619, 968
- Wu, X. F., Dai, Z. G., Huang, Y. F., & Lu, T. 2003, MNRAS, 342, 1131
- Wu, X. F., Dai, Z. G., Wang, X. Y., et al. 2007, Advances in Space Research, 40, 1208
- Wu, X. F., Dai, Z. G., Wang, X. Y., et al. 2006, 36th COSPAR Scientific Assembly, 36, 731
- Yi, S. X., Wu, X. F., & Dai, Z. G. 2013, ApJ, 776, 120
- Yi, S. X., Lei, W. H., Zhang, B., Dai, Z. G., Wu, X. F., & Liang, E. W. 2015, ApJ, submitted
- Zhang, B., Fan, Y. Z., Dyks, J., et al. 2006, ApJ, 642, 354
- Zhang, B., & Mészáros, P. 2004, Int. J. Mod. Phys. A., 19, 2385

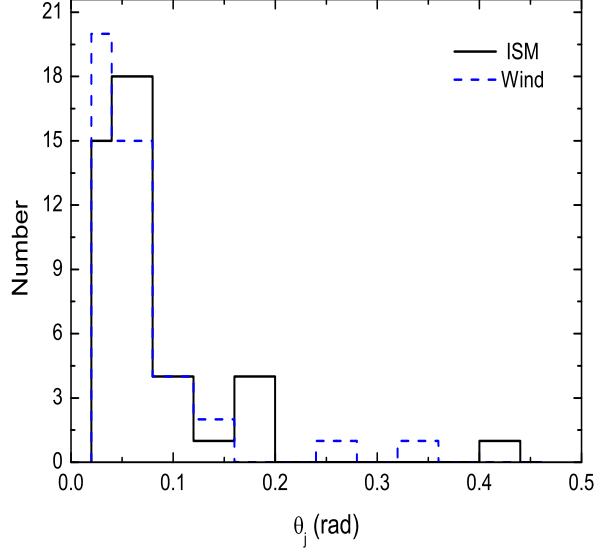


Fig. 1.— The distribution of half-opening angles of GRB jets. The solid and dash lines are corresponding to the ISM and wind cases, respectively.

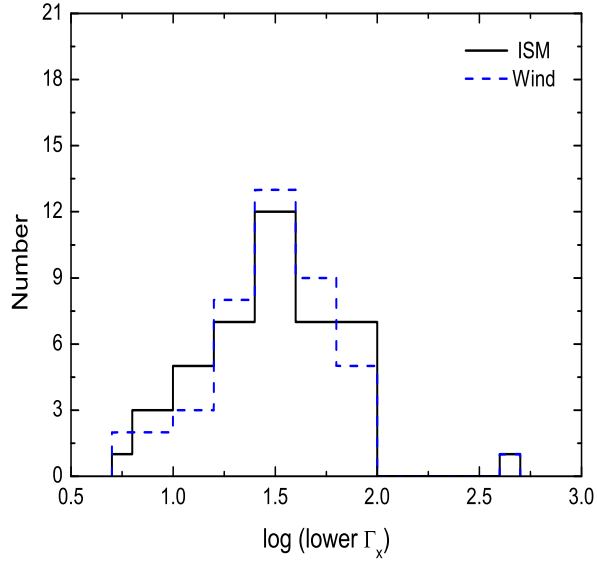


Fig. 2.— The distribution of the lower limits on the Lorentz factor of X-ray flares for two types of circumburst environment. The lower limits on Γ_x range from tens to a few hundreds for the ISM (solid) and wind (dashed) cases.

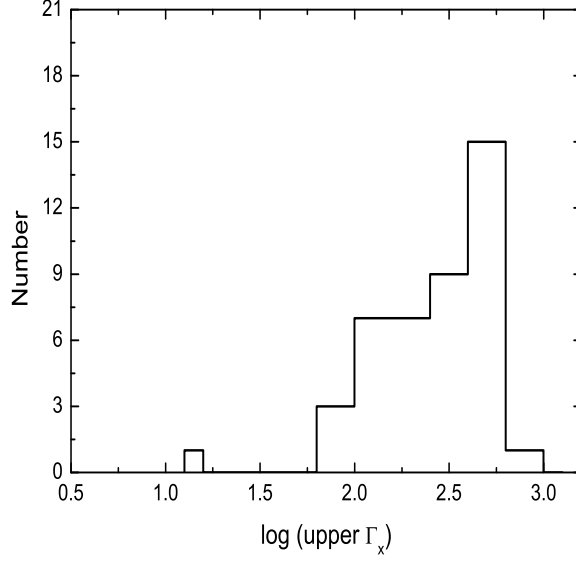


Fig. 3.— The distribution of the upper limits on the X-ray flare Lorentz factor.

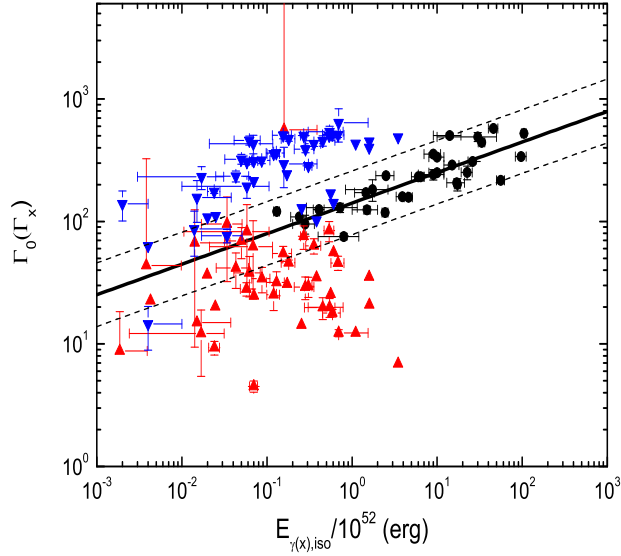


Fig. 4.— Lorentz factor and isotropic radiation energy of X-ray flares (rest frame 0.3-10 keV, triangles) and prompt GRBs (solid dots) for the ISM case. The best fit power-law index of the correlation for prompt GRBs is 0.25.

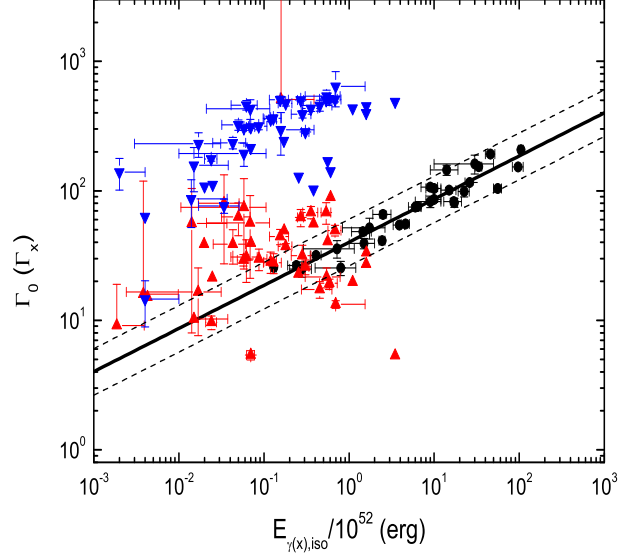


Fig. 5.— Lorentz factor and isotropic radiation energy of X-ray flares (rest frame 0.3-10 keV, triangles) and prompt GRBs (solid dots) for the wind case. The best fit power-law index of the correlation for prompt GRBs is 0.33.

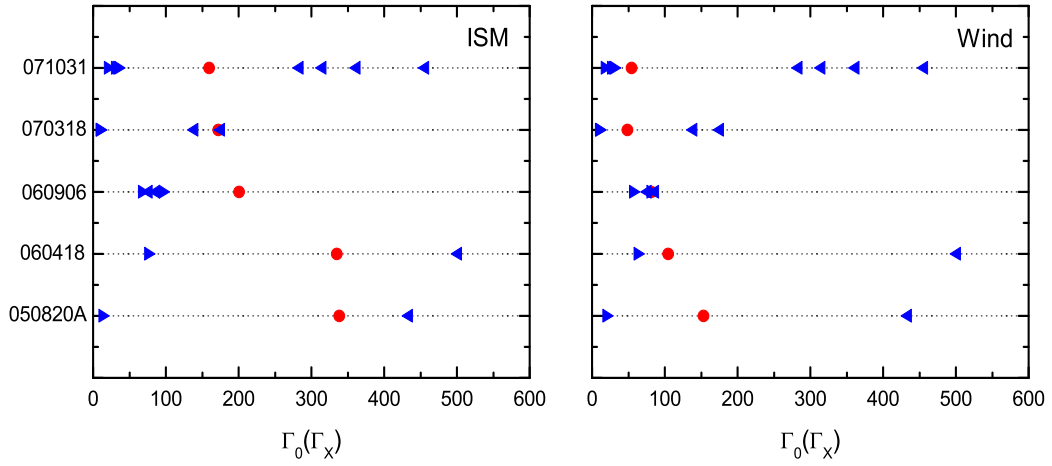


Fig. 6.— Prompt (solid dots) and X-ray flare (triangles) Lorentz factors of 5 GRBs.

Table 1. Properties of GRB X-ray Flares

GRB	z	T_{rise} (s)	T_{decay} (s)	S_x (10^{-7} erg cm $^{-2}$)	$T_{90,x}$ (s)	$E_{x,iso,50}$ (10^{50} erg)	θ_J^{ISM} (rad)	θ_J^{Wind} (rad)	Lower Γ_x^{ISM}	Lower Γ_x^{Wind}	Upper Γ_x
050416A	0.650	2.2E5 \pm 2.8E6	2.8E5 \pm 5.8E5	0.34 \pm 0.53	5.0E5	0.4 \pm 0.6	0.026 \pm 0.005	0.071 \pm 0.009	43.7 \pm 281.9	15.9 \pm 102.7	14.6 \pm 5.7
050802	1.710	123.0 \pm 0	22.0 \pm 0	0.20 \pm 0.30	145.0	1.5 \pm 2.3	0.028 \pm 0.002	0.041 \pm 1E-3	14.9 \pm 0	10.3 \pm 0	157.1 \pm 58.9
050814 (1)	5.300	217.0 \pm 0	624.0 \pm 0	0.04 \pm 0	841.0	2.0 \pm 0	0.046 \pm 0.003	0.044 \pm 0.002	36.6 \pm 0	38.7 \pm 0	108.5 \pm 0
050814 (2)	5.300	505.0 \pm 0	439.0 \pm 0	0.05 \pm 0	944.0	2.5 \pm 0	0.046 \pm 0.003	0.044 \pm 0.002	20.1 \pm 0	21.3 \pm 0	111.4 \pm 0
050820A	2.620	34.0 \pm 0	148.0 \pm 0	6.89 \pm 0	182.0	110.5 \pm 0	0.169 \pm 0.007	0.106 \pm 0.003	12.3 \pm 0	19.7 \pm 0	434.5 \pm 0
050904 (1)	6.290	120.0 \pm 0	107.0 \pm 0	2.51 \pm 0	227.0	160.3 \pm 0	0.045 \pm 0.007	0.028 \pm 0.003	20.8 \pm 0	33.2 \pm 0	451.3 \pm 0
050904 (2)	6.290	96.0 \pm 0	188.0 \pm 0	0.27 \pm 0	284.0	17.2 \pm 0	0.045 \pm 0.007	0.028 \pm 0.003	30.9 \pm 0	49.2 \pm 0	244.4 \pm 0
050904 (3)	6.290	86.0 \pm 0	108.0 \pm 0	0.11 \pm 0	194.0	7.0 \pm 0	0.045 \pm 0.007	0.028 \pm 0.003	24.7 \pm 0	39.4 \pm 0	214.7 \pm 0
050904 (4)	6.290	1680.0 \pm 0	2236.0 \pm 0	0.88 \pm 0	3916.0	56.2 \pm 0	0.045 \pm 0.007	0.028 \pm 0.003	25.4 \pm 0	40.6 \pm 0	170.4 \pm 0
050904 (5)	6.290	1176.0 \pm 0	7537.0 \pm 0	0.95 \pm 0	8713.0	60.7 \pm 0	0.045 \pm 0.007	0.028 \pm 0.003	55.9 \pm 0	89.1 \pm 0	142.2 \pm 0
050904 (6)	6.290	5773.0 \pm 0	14457.0 \pm 0	0.60 \pm 0	20230.0	38.3 \pm 0	0.045 \pm 0.007	0.028 \pm 0.003	34.9 \pm 0	55.7 \pm 0	102.7 \pm 0
050904 (7)	6.290	3774.0 \pm 0	1586.0 \pm 0	0.40 \pm 0	5360.0	25.6 \pm 0	0.045 \pm 0.007	0.028 \pm 0.003	14.3 \pm 0	22.8 \pm 0	129.3 \pm 0
051016B	0.940	109.0 \pm 0	1457.0 \pm 0	0.18 \pm 0	1566.0	0.4 \pm 0	0.162 \pm 0.039	0.242 \pm 0.039	22.6 \pm 0	15.1 \pm 0	63.3 \pm 0
060115	3.530	19.1 \pm 10.2	64.3 \pm 9.3	0.17 \pm 0.07	83.4	4.3 \pm 1.8	0.044 \pm 0.007	0.047 \pm 0.005	41.8 \pm 13.4	38.7 \pm 11.5	234.5 \pm 24.1
060124 (1)	2.300	291.0 \pm 0	70.0 \pm 0	27.13 \pm 0	361.0	347.5 \pm 0	0.071 \pm 0.005	0.092 \pm 0.005	6.9 \pm 0	5.3 \pm 0	487.6 \pm 0
060124 (2)	2.300	50.0 \pm 0	313.0 \pm 0	12.40 \pm 0	363.0	158.8 \pm 0	0.071 \pm 0.005	0.092 \pm 0.005	35.2 \pm 0	27.2 \pm 0	400.3 \pm 0
060210 (1)	3.910	23.1 \pm 1.5	37.6 \pm 2.1	2.30 \pm 0.40	60.7	68.4 \pm 11.9	0.028 \pm 0.003	0.026 \pm 0.002	45.9 \pm 6.1	49.4 \pm 4.6	507.1 \pm 22.0
060210 (2)	3.910	14.7 \pm 1.8	45.5 \pm 3.2	1.20 \pm 0.24	60.2	35.7 \pm 7.1	0.028 \pm 0.003	0.026 \pm 0.002	63.3 \pm 9.1	68.1 \pm 7.4	431.9 \pm 21.6
060418	1.490	5.6 \pm 0.5	19.5 \pm 0.5	4.80 \pm 0.40	25.0	27.0 \pm 2.3	0.025 \pm 0.005	0.030 \pm 0.004	75.6 \pm 16.6	62.2 \pm 9.3	501.9 \pm 10.5
060526 (1)	3.220	11.8 \pm 0.6	12.7 \pm 1.6	3.20 \pm 3.90	24.5	69.6 \pm 84.9	0.0850 \pm 7.891E-4	0.0780 \pm 4.86E-4	12.3 \pm 0.8	13.3 \pm 0.9	639.1 \pm 194.7
060526 (2)	3.220	9.8 \pm 1.6	27.9 \pm 8.6	2.50 \pm 1.10	37.8	54.4 \pm 23.9	0.0850 \pm 7.891E-4	0.0780 \pm 4.86E-4	20.0 \pm 3.5	21.6 \pm 3.8	539.1 \pm 59.3
060526 (3)	3.220	15.2 \pm 1.2	34.6 \pm 4.3	2.70 \pm 0.63	49.9	58.7 \pm 13.7	0.0850 \pm 7.891E-4	0.0780 \pm 4.86E-4	17.9 \pm 1.3	19.3 \pm 1.4	512.7 \pm 29.9
060526 (4)	3.220	10.2 \pm 4.2	61.7 \pm 3.7	1.30 \pm 0.34	71.9	28.3 \pm 7.4	0.0850 \pm 7.891E-4	0.0780 \pm 4.86E-4	29.1 \pm 6.1	31.5 \pm 6.6	389.8 \pm 25.5
060707	3.425	8.1 \pm 8.0	26.5 \pm 10.0	0.07 \pm 0.06	34.6	1.7 \pm 1.4	0.149 \pm 0.024	0.110 \pm 0.012	12.2 \pm 6.7	16.5 \pm 8.9	231.3 \pm 49.6
060714 (1)	2.711	8.1 \pm 3.0	41.6 \pm 2.0	3.30 \pm 0.43	49.6	53.9 \pm 7.0	0.0270 \pm 8.414E-4	0.0330 \pm 6.938E-4	84.2 \pm 15.9	68.0 \pm 12.8	502.7 \pm 16.4
060714 (2)	2.711	4.0 \pm 2.1	4.2 \pm 2.1	0.38 \pm 0.13	8.2	6.2 \pm 2.1	0.0270 \pm 8.414E-4	0.0330 \pm 6.938E-4	38.1 \pm 13.9	30.8 \pm 11.2	459.2 \pm 39.3
060714 (3)	2.711	4.4 \pm 1.1	9.6 \pm 1.0	0.95 \pm 0.24	14.0	15.5 \pm 3.9	0.0270 \pm 8.414E-4	0.0330 \pm 6.938E-4	54.9 \pm 7.6	44.4 \pm 6.1	505.2 \pm 31.9
060714 (4)	2.711	8.3 \pm 0.6	12.8 \pm 0.5	1.10 \pm 0.20	21.1	18.0 \pm 3.3	0.0270 \pm 8.414E-4	0.0330 \pm 6.938E-4	46.1 \pm 2.4	37.3 \pm 1.7	473.0 \pm 21.5
060729	0.540	9.6 \pm 1.0	34.1 \pm 2.0	9.30 \pm 1.00	43.7	7.0 \pm 0.8	0.418 \pm 0.037	0.350 \pm 0.020	4.5 \pm 0.5	5.4 \pm 0.5	311.3 \pm 8.4
060814	0.840	9.3 \pm 1.3	29.7 \pm 2.3	3.10 \pm 0.48	39.0	5.8 \pm 0.9	0.064 \pm 0.006	0.061 \pm 0.004	28.1 \pm 3.5	29.2 \pm 3.0	305.2 \pm 11.8
060906 (1)	3.690	349.0 \pm 397.0	1110.0 \pm 1420.0	0.05 \pm 0.08	1460.0	1.4 \pm 2.3	0.027 \pm 0.002	0.032 \pm 1E-3	66.9 \pm 57.4	56.0 \pm 48.0	86.8 \pm 34.7
060906 (2)	3.690	774.0 \pm 987.0	5030.0 \pm 1640.0	0.12 \pm 0.06	5810.0	3.4 \pm 1.7	0.027 \pm 0.002	0.032 \pm 1E-3	95.6 \pm 63.3	80.1 \pm 52.9	76.5 \pm 9.6
070306	1.500	8.7 \pm 1.4	34.7 \pm 3.3	2.10 \pm 0.35	43.4	12.0 \pm 2.0	0.079 \pm 0.019	0.071 \pm 0.011	25.3 \pm 6.6	28.3 \pm 5.3	356.8 \pm 14.9
070318 (1)	0.840	9.5 \pm 16.2	19.4 \pm 26.1	0.10 \pm 0.11	28.9	0.2 \pm 0.2	0.163 \pm 0.011	0.157 \pm 0.007	8.8 \pm 9.6	9.1 \pm 9.9	139.4 \pm 38.3
070318 (2)	0.840	44.9 \pm 8.3	103.0 \pm 12.6	1.30 \pm 0.19	147.9	2.4 \pm 0.4	0.163 \pm 0.011	0.157 \pm 0.007	9.3 \pm 1.2	9.6 \pm 1.1	176.0 \pm 6.4
070721B (1)	3.626	0.9 \pm 145.7	120.8 \pm 149.1	0.60 \pm 0.87	121.7	15.8 \pm 23.0	0.0210 \pm 7.033E-4	0.0230 \pm 5.182E-4	561.6 \pm 45459.9	508.2 \pm 41133.9	295.7 \pm 107.2
070721B (2)	3.626	4.4 \pm 4.4	7.3 \pm 5.5	0.26 \pm 0.18	11.7	6.9 \pm 4.8	0.0210 \pm 7.033E-4	0.0230 \pm 5.182E-4	62.4 \pm 39.1	56.5 \pm 35.4	430.8 \pm 74.6
070721B (3)	3.626	8.9 \pm 4.0	18.3 \pm 6.3	0.19 \pm 0.07	27.2	5.0 \pm 1.8	0.0210 \pm 7.033E-4	0.0230 \pm 5.182E-4	69.5 \pm 19.8	62.9 \pm 17.9	322.6 \pm 29.7
070721B (4)	3.626	62.2 \pm 64.3	179.8 \pm 151.2	0.22 \pm 0.18	242.0	5.8 \pm 4.8	0.0210 \pm 7.033E-4	0.0230 \pm 5.182E-4	82.4 \pm 55.0	74.6 \pm 49.7	193.7 \pm 39.6
071031 (1)	2.690	25.0 \pm 3.5	36.2 \pm 2.6	2.80 \pm 1.10	61.2	45.2 \pm 17.8	0.061 \pm 0.011	0.069 \pm 0.009	19.8 \pm 4.0	17.3 \pm 2.5	456.4 \pm 44.8
071031 (2)	2.690	9.3 \pm 1.9	34.7 \pm 5.0	0.80 \pm 0.19	44.0	12.9 \pm 3.1	0.061 \pm 0.011	0.069 \pm 0.009	31.8 \pm 7.1	27.8 \pm 4.9	362.4 \pm 21.5
071031 (3)	2.690	9.8 \pm 2.4	42.1 \pm 6.3	0.54 \pm 0.13	51.9	8.7 \pm 2.1	0.061 \pm 0.011	0.069 \pm 0.009	34.1 \pm 8.0	29.8 \pm 5.7	315.2 \pm 19.0
071031 (4)	2.690	65.5 \pm 4.4	210.6 \pm 9.0	1.90 \pm 0.19	276.1	30.7 \pm 3.1	0.061 \pm 0.011	0.069 \pm 0.009	29.5 \pm 5.6	25.8 \pm 3.3	284.3 \pm 7.1